International Journal of Heat and Mass Transfer 179 (2021) 121718

Contents lists available at ScienceDirect

International Journal of Heat and Mass Transfer

journal homepage: www.elsevier.com/locate/hmt

Transient liquid crystal thermography using a time varying surface heat flux

Julian Schmid[a,b,1,*], Michele Gaffuri[a,1,*], Alexandros Terzis[c], Peter Ott[a], Jens von Wolfersdorf[b]

[a] Group of Thermal Turbomachinery (GTT), EPFL - Swiss Federal Institute of Technology, 1015 Lausanne, Switzerland
[b] Institute of Aerospace Thermodynamics (ITLR), University of Stuttgart, 70569 Stuttgart, Germany
[c] Faculty of Aerospace Engineering, Technion Israel Institute of Technology, 3200003 Haifa, Israel

ARTICLE INFO

Article history:
Received 22 January 2021
Revised 1 July 2021
Accepted 9 July 2021

Keywords:
Transient heat transfer measurement
Thermochromic liquid crystals
Jet impingement
Heater foil

ABSTRACT

Heat transfer measurements are required in a wide range of fields, for example to validate new cooling concepts in turbomachinery, to assess the performances of heat exchangers, and to provide data for numerical simulations. Thereby transient methods are often applied for local heat transfer resolution. A particular challenge is posed by complex flows, where the determination of the heat transfer coefficients with the commonly applied transient heater mesh method can prove difficult, for instance in cases in which the flow can take different paths leading to mixing flows at different temperatures, and a difficult determination of the reference temperature. One way to address these complex systems is the transient heater foil method, in which the experiment is driven by a constant heat flux generated at the surface under study, instead of a temperature variation in the flow. However, the accuracy of the measurement remains an open issue compared to the heater mesh method. Here we show a modification of the heater foil method, which uses a linearly increasing surface heat flux to improve the measurement accuracy, especially in the low heat transfer regions. The new method is validated by measuring the heat transfer of a single circular jet perpendicularly impinging on a flat plate, and by comparing the results to a correlation available in the literature. Results show good agreement with the literature, while providing considerable accuracy improvement with respect to the heater foil method with constant heat flux. The heater foil method presented here, reaches similar uncertainty values as the state of the art versions of the heater mesh method in low heat transfer regions, while providing better accuracy in the high heat transfer regions. Additionally, it allows for an easier implementation for certain problems, provided that optical access is guaranteed and the surface curvature allows for the addition of the heater foil.

1. Introduction

Thanks to the achievable spatial resolution and low intrusiveness, thermochromic liquid crystals have been extensively used for the determination of the convective heat transfer coefficient of a fluid heating or cooling [1] a solid, and to characterize the performances of heat exchangers [2] and cooling systems of gas turbine blades (e.g. [3]). Other important applications include the determination of the film cooling effectiveness [4–6] and the measurement of the surface shear stresses [7,8].

Many studies apply heater foils on low conducting materials to obtain local heat transfer data via wide- or narrow-band thermochromic liquid crystals (TLC) [9–13], infrared thermography [14–16] or temperature sensitive paint (TSP) [17,18] in steady state experiments. By considering appropriately the heat losses and lateral conduction effects (e.g. [19–21]) low uncertainty (about 5–8%) in the obtained heat transfer coefficients can be achieved. Less frequently, heat is provided by keeping the opposite side of the solid at an uniform temperature via a liquid bath [22–24].

Alternatively, with such an experimental setup, transient measurements can also be performed by instantaneously powering the heater foil, but this generally leads to higher uncertainties due to the additional transient effects. Instead, transient methods usually rely on a step change of the flow temperature [25–27], and the time required to reach a certain color of the liquid crystals allows for the determination of the heat transfer coefficient, usually

* Corresponding authors.
E-mail addresses: julschmid@ethz.ch (J. Schmid), michele.gaffuri@epfl.ch (M. Gaffuri).
[1] These authors contributed equally to this work.

https://doi.org/10.1016/j.ijheatmasstransfer.2021.121718

Nomenclature

A	jet area, $[mm^2]$
A_F	foil area, $[m^2]$
C_D	discharge coefficient, [-]
c_p	specific heat at constant pressure, $[J/(K\,kg)]$
D	jet hole diameter, $[mm]$
h	heat transfer coefficient, $[W/(m^2\,K)]$
I	Current, $[A]$
k_f	fluid thermal conductivity, $[W/m\,K]$
k	thermal conductivity, $[W/m\,K]$
L/D	length-to-diameter ratio, [-]
$\dot{m}$	mass flow, $[kg/s]$
$Nu_D = h\,D/k_f$	Nusselt number, [-]
Δp	pressure difference, $[Pa]$
q	heat flux, $[W/m^2]$
q_0	increase of heat flux, $[W/(m^2\,s)]$
q_{ti}	heat flux thermal inertia, $[W/m^2]$
q_l	heat flux lateral conduction, $[W/m^2]$
r/D	radial distance, [-]
Re_D	Reynolds number, [-]
T	temperature, $[K]$
T_0	ambient/initial temperature, $[K]$
T_{aw}	adiabatic wall temperature, $[K]$
T_g	jet temperature, $[K]$
T_{LC}	liquid crystal indication temperature, $[K]$
T_r	recovery temperature, $[K]$
t	time, $[s]$
t_{LC}	liquid crystal indication time, $[s]$
U	Voltage drop, $[V]$
z	depth coordinate, $[mm]$
Z/D	jet-to-plate distance, [-]

Greek letters

α	thermal diffusivity, $[m^2/s]$
α_T	temperature coefficient, $[1/K]$
Δ	relative uncertainty, [-]
δ	foil thickness, $[mm]$
ρ_f	fluid density, $[kg/m^3]$
ρ_s	solid density, $[kg/m^3]$
η	adiabatic wall effectiveness, [-]
σ	standard deviation
μ	dynamic viscosity, $[kg/m\,s]$

Abbreviations

DC	direct current
HTC	Heat transfer coefficient
PMMA	Poly(methyl methacrylate)
CCD	charge-coupled device
TSP	temperature sensitive paint
TLC	thermochromic liquid crystals

assuming one dimensional heat conduction into a semi-infinite solid (provided that the assumption is sound [28,29]), although corrections for lateral conduction have been proposed [30–33]. Methodologies for more complex temperature evolutions have also been developed: a series of steps can be assumed (using Duhamel principle) to account for the temperature evolution at the beginning of the experiment which differs from an ideal step [34,35]; alternatively, a ramp [36] or a series of ramps can be prescribed, which can improve the accuracy of the method. Analytical solutions of the heat equation for flow temperature evolutions described as polynomials [37] or as a sum of exponentials [38] have been obtained; these allow to better approximate the real temperature evolution.

An interesting approach for a transient technique with a surface heat flux has been proposed by von Wolfersdorf et al. [39], in which a constant heat flux is applied for a certain time until the region of interest reaches a temperature higher than the liquid crystal color temperature, followed by a lower constant heat flux. This allows for the determination of the heat transfer coefficient without knowledge of the local surface heat flux, which can be non uniform. More recently, a method using a constant heat flux has been developed [40], which essentially implements the first part of the method in [39] and needs knowledge of the applied heat flux, which must be uniform. This latter method suffers from low accuracy in the low heat transfer regions when a wide range of heat transfer coefficients has to be measured, since the heat flux needed to reach the liquid crystal temperature in the high heat transfer regions results in a very short appearance time of the liquid crystals in the low heat transfer regions. Despite this drawback, a transient method using a surface heat flux is appealing because it avoids several problems associated with a flow temperature based approach: *i)* the step change is almost ideal, which facilitates the implementation by eliminating the need for redirecting the hot flow or accounting for the thermal inertia of the heater mesh [41] and thermocouples [42], and *ii)* the flow is kept at ambient temperature, eliminating the problem of the determination of the driving gas temperature, which can be a difficult task in complex flows, especially when mixing processes occur, for example in a multi-channel device with bypasses between channels.

In this paper an improvement of this method is reported, in which the heat flux is linearly increased; this allows for an increased accuracy in low heat transfer regions. An analytical solution of the one dimensional, semi-infinite heat equation for this problem is provided. The technique was used for the determination of the heat transfer coefficient of a jet impinging on a flat surface with a distance between 4 and 10 jet diameters and Reynolds numbers, based on the jet diameter, between 20000 and 40000. This problem has been chosen because of the wide range of heat transfer coefficients achieved on the target plate, and the availability of experimental data for validation. In particular, results are compared to the correlation of Goldstein and Franchett [24] to validate the method. An assessment of the effects of thermal inertia and lateral conduction in the foil is presented. Finally, an extension of Goldstein and Franchett's correlation for arbitrary jet to plate distances between 4 and 10 jet diameters is proposed in Appendix D.

2. Transient heater foil method

The target plate, made of a transparent material with low thermal diffusivity α and low thermal conductivity k (usually PMMA) is coated with thermochromic liquid crystals and black paint, on which a thin metallic foil is attached to provide a surface heat flux. The liquid crystals, the black paint and the glue used to attach the foil to the surface are considered to have similar thermal properties as the plate material, so that a single material can be assumed. Additionally, the glue used provides good surface wetting, so that thermal resistance between the various layers can be neglected. At the beginning of the experiment a time-varying heat flux $q(t)$ is applied to the surface. In this implementation, the flux has a linear evolution: $q(t) = q_0 t$, where q_0 is the rate of increase of the heat flux. The evolution of the liquid crystals on the target plate is observed using a CCD camera, and the time t_{LC} required for each pixel to reach the maximum green intensity (corresponding to the temperature T_{LC}) is determined from the video.

To find the heat transfer coefficient at each point, the one-dimensional heat conduction equation is considered:

$$\frac{\partial^2 T(z,t)}{\partial z^2} = \frac{1}{\alpha}\frac{\partial T(z,t)}{\partial t} \tag{1}$$

Suitable initial and boundary conditions are needed. The plate is initially at ambient temperature:

$$T(z, t = 0) = T_0 \tag{2}$$

If the relationship between the plate thickness δ and the experiment time is such that $\delta > 2\sqrt{\alpha t}$, the plate can be assumed to be semi-infinite [29], leading to the following boundary condition:

$$T(z \to \infty, t) = T_0 \tag{3}$$

At the surface, the heat flux is equal to the heat convected into the flow and the heat conducted into the plate, which can be expressed in the boundary condition as follows:

$$-k\frac{\partial T(0, t > 0)}{\partial z} - h[T_{aw} - T(0, t)] = q_0 t \tag{4}$$

Radiation effects are neglected because the temperatures involved are low (the indication temperature of the liquid crystals used is 38 °C); the heat required to heat the metallic foil can also be neglected and the validity of this assumption is analyzed later in the paper. In Eq. (4), the term T_{aw} is the adiabatic wall temperature, which can be considered equal to the initial temperature T_0 if the jet is at ambient condition. If not, as is the case here, where the fan motor raises the jet temperature ($T_g \neq T_0$) by about 5–10K depending on the flow condition, T_{aw} must be determined considering the entrainment effect that mixes the jet at temperature T_g and the surrounding air at temperature T_0. To determine both unknowns, heat transfer coefficient h and adiabatic wall temperature distributions T_{aw}, several approaches have been taken in the literature. Thereby multiple TLC- indications in one transient test (e.g. [43]), different temperature mixing situations (e.g. [44]) or different levels for step-heating of heater foils (e.g [4,6]) in multiple film cooling tests with associated regression analysis methods in the data reduction might be applied. Alternatively, combinations of steady state (heater foil) and transient (heater mesh) experiments using TLC as temperature indicator have been used (e.g. [45]). To simplify this aspect in the present work for comparison of different heating conditions an entrainment effect correlation [46] is applied to determine T_{aw} thereby prescribing the same flow temperature conditions for the different heating situations. The entrainment η effect is defined as:

$$\eta = \frac{T_{aw} - T_r}{T_g - T_0} \tag{5}$$

where T_r is the recovery temperature, which is defined as the adiabatic wall temperature T_{aw} when the jet total temperature is equal to the ambient temperature. In the present work, the recovery temperature T_r is assumed to be equal to the ambient temperature T_0, similarly to [47]; the potential error of this simplification is negligible due to the low jet Mach number ($M_{\max} \approx 0.1$). In order to fulfill the initial condition Eq. (2), which implies that the model is initially at ambient temperature T_0, the jet is redirected and hits the target plate first at time t=0.

With these assumptions Eq. (1) can be solved using the Laplace transform method (see Appendix B for detailed resolution steps), leading to the following expression:

$$\begin{aligned} T(z,t) - T_0 = (T_{aw} - T_0)&\left[\operatorname{erfc}(a) - \mathrm{e}^b \operatorname{erfc}(a+c)\right] \\ &+ \frac{q_0}{k\alpha^2}\left[\frac{\alpha}{(-\frac{h}{k})^3}\mathrm{e}^b \operatorname{erfc}(a+c)\right. \\ &\left. - \frac{\alpha}{(-\frac{h}{k})^3}\sum_{r=0}^{2}(-2c)^r i^r \operatorname{erfc}(a)\right] \end{aligned} \tag{6}$$

where $a = \frac{z}{2\sqrt{\alpha t}}$, $b = \frac{hz}{k} + \alpha t \frac{h^2}{k^2}$, and $c = \frac{h}{k}\sqrt{\alpha t}$ are introduced to simplify the expression. In Eq. (6), the term $i^r \operatorname{erfc}(a)$ denotes the rth successive integration of the complementary error function, which can be defined iteratively as follows (see Appendix 2 in [48]):

$$i^n \operatorname{erfc}(x) = \int_x^\infty i^{n-1}\operatorname{erfc}(\xi)\, d\xi \tag{7}$$

$$i^0 \operatorname{erfc}(x) = \operatorname{erfc}(x) \tag{8}$$

If the time $t = t_{LC}$ required to reach the liquid crystal indication temperature T_{LC} is known, the heat transfer coefficient h can be calculated pixel-wise numerically using Eq. (6), by setting the depth z to the thickness of the black paint and glue, provided that the thermal properties of the material are known. For this paper, the maximum green intensity of low bandwidth liquid crystals is considered for T_{LC}, but in principle one could also use higher bandwidth liquid crystals and consider their hue evolution in time to get more data points and find the value h for which Eq. (6) best fits the temperature evolution. The latter approach however would require an accurate calibration of the hue-temperature curve, which is very sensitive to changes in illumination and view angle.

Equation (6) can be further simplified in cases where the gas temperature is equal to the ambient temperature, so that $T_{aw} = T_0$:

$$\begin{aligned} T(z,t) \quad &= T_0 + \frac{q_0}{k\alpha^2}\left[\frac{\alpha}{(-\frac{h}{k})^3}\mathrm{e}^b \operatorname{erfc}(a+c)\right. \\ &\left. - \frac{\alpha}{(-\frac{h}{k})^3}\sum_{r=0}^{2}(-2c)^r i^r \operatorname{erfc}(a)\right] \end{aligned} \tag{9}$$

To illustrate the appeal of the method, Fig. 1 shows the relationship between the measured time and the heat transfer coefficient using Eq. (9), and the corresponding curve for the step method as applied in [40], for the following conditions: PMMA material properties, T_0 = 20 °C, T_{LC} = 38 °C, z=0, and heat flux conditions set to have an experiment duration of two minutes for a heat transfer coefficient of $300 W/m^2$K.

The ramp method provides an almost linear relationship between these parameters, which is the optimal relationship between the measured variable (in this case the time) and the derived variable of interest (in this case the heat transfer coefficient). In contrast, the step method has a very large gradient at low heat transfer coefficients, which means that a small error in the time determination leads to a large error in the derived heat transfer coefficient. At the other end of the spectrum, the step method reaches a plateau, and higher heat transfer coefficients cannot be determined, no matter how long the experiment lasts. The ramp method is more flexible: the heat flux keeps increasing, higher

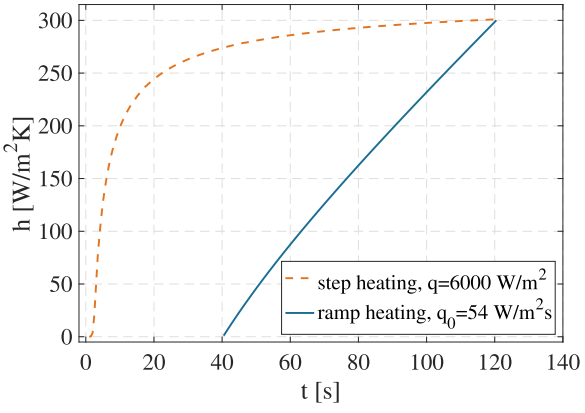

Fig. 1. Relationship between liquid crystal indication time and heat transfer coefficient for the transient step heating method [40] (dashed line), and the ramp method presented in this paper (solid line).

heat transfer coefficients can be tested simply by running the experiment for a longer time, provided that the maximum allowed temperature for the material is not reached and the condition for the semi-infinite assumption is still valid ($t < \delta^2/4\alpha$).

It must be pointed out that, in order to apply this method, the part to be analysed must have fairly regular and possibly low surface curvature, so that the metallic heater foil used to generate the surface heat flux can effectively be attached to the surface. As an example of the surface curvature for which this method could be used, there have been implementations of the heater foil method for the analysis of film cooling in turbine blades [4]. The application of thin films via vapor metal deposition [49,50] could tackle more complex geometries; however, for internal channels, optical access must be guaranteed and this is the main limitation. Heat transfer enhancing features like pin-fins or ribs can be installed on top of the foil, provided that the latter has a low temperature coefficient, so that the temperature change caused by the augmentation device does not alter the local resistivity of the foil. Additionally, an approach similar to Tran and Kapat [51] could be used to estimate the performance of the rib or pin-fin itself.

3. Experimental setup

3.1. Low speed wind-tunnel

The impingement test facility used for this work is depicted in Fig. 2. It consists of an open-circuit, low-speed wind tunnel operated in blowing mode using two counter-rotating axial fans. A settling chamber with honeycombs, a convergent bell mouth and a straight square section (100 mm side) complete the wind tunnel. A 15 mm thick jet plate is mounted at the end of the tunnel. The large hole diameter was mainly chosen in order to increase the spatial magnification ($pixel/D$) in the measurement and to avoid compressibility effects [52]. The jet hole has a diameter D=15 mm resulting in a nozzle of length-to-diameter ratio equal to one (L/D=1). The jet hole is chamfered on both sides (30° × 1 mm). The target plate is mounted on four threaded rods to adjust the jet-to-plate distance Z/D.

3.2. Test model

A schematic layered representation of the surface to be examined is shown in Fig. 3. A transparent PMMA plate (20 mm thick) is painted with thermochromic liquid crystals (Hallcrest R38C1W) and black paint (Hallcrest SPB 100). The liquid crystals have a narrow band of 1 °C, which allows for a very precise temperature indication. The thickness of the paint layer, measured with an Elcometer Coating Thickness Gauge, was 10±1 μm; it is important to consider this thickness when evaluating the results, as highlighted in [53] and [54]. A 30 μm thick foil made of a low temperature coefficient iron-chromium-aluminium alloy (1.4767 $\alpha_T = 0.0193 \times 10^{-3}$ K^{-1}) is bonded to the black paint with a highly thermally conductive adhesive tape (3M 8805). At the lateral ends, the foil is clamped between copper bars to ensure a uniform current flow across the foil. The low temperature coefficient ensures that the resistivity of the material can be considered constant in the temperature range of the tests (i.e. from ambient temperature to approximately 70 °C, the resistivity change is about 0.1%). The available area of the heat transfer coefficient evaluation is limited to r/D=5 to reduce possible disturbance influences of the threaded rods holding the target plate. A schematic front view of the target plate is shown in Fig. 2.

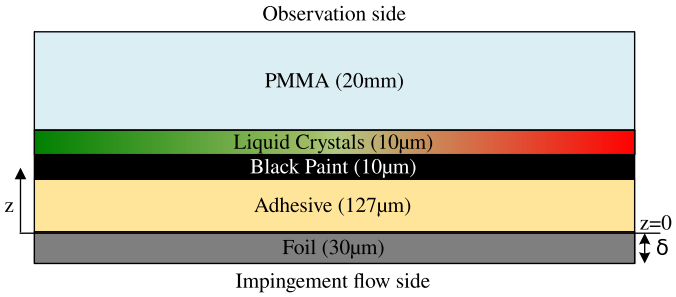

Fig. 3. Schematic layered representation of the surface to be examined, layer thicknesses not to scale.

The liquid crystals are calibrated using a procedure similar to Waidmann et al. [55]. A temperature gradient is generated in a thermally insulated copper bar by keeping its ends at different temperatures. Calibrated thermocouples embedded in the copper bar provide temperature information at various locations. One side of the bar is covered with liquid crystals so that a relationship between local temperature and liquid crystal color can be determined.

3.3. Instrumentation

Type K thermocouples are mounted upstream of the orifice plate inside the tunnel to evaluate the jet temperature. The ambient temperature was determined close to the target plate, ensuring no influence of the jet. All used thermocouples were calibrated together in a temperature controlled liquid bath (Lauda E4S) using a precision resistance thermometer resulting in a maximum deviation of 0.1K.

The mass flow was determined by means of the discharge coefficient using the difference between the pressure upstream of the jet and the ambient pressure.

$$\dot{m} = C_d A \sqrt{2\rho_f \Delta p} \tag{10}$$

where A is the jet area, and the discharge coefficient C_d was determined a priori by measuring jet velocity profiles with a

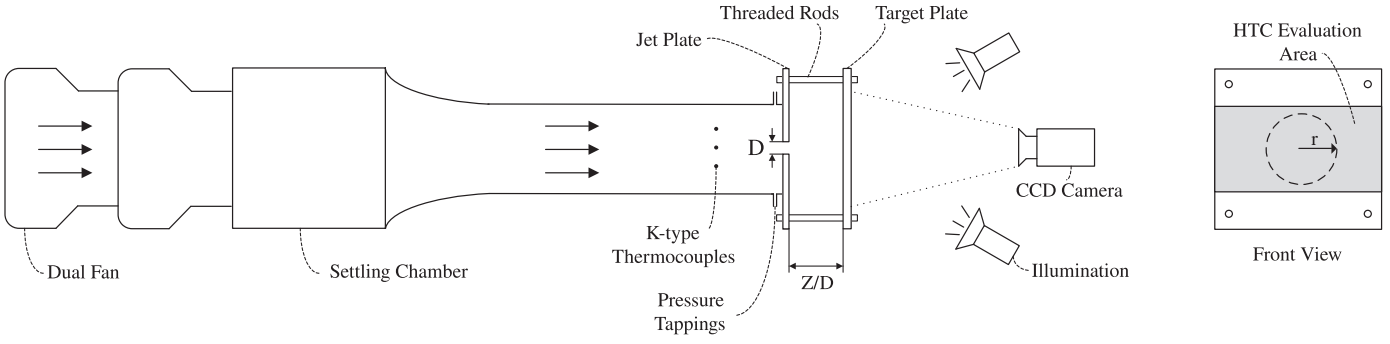

Fig. 2. Schematic representation of the experimental setup and front view of the target plate.

traversing Pitot tube and Δp at various mass flows (see Appendix A). The scanner used for pressure measurements has an accuracy of ± 8 *Pa*.

The Reynolds number, based on the jet diameter, follows directly from Eq. (10):

$$Re_D = C_d D \frac{\sqrt{2\rho_f \Delta p}}{\mu} \tag{11}$$

The accuracy of the Reynolds number determination was estimated at or below 4%, similar to previous experiments carried out on this setup [56].

The electrical power required to use the heater foil as a surface energy source is provided by a DC power supply in voltage control mode, capable of reaching a maximum voltage and current of 40 *V* and 128 *A*. The voltage drop *U* across the foil was measured at the copper bars. A shunt resistor in series with the foil is used to ensure accurate determination of the current flow *I*, by measuring the voltage drop across the resistor. The rate of increase of heat flux q_0 to solve Eq. (6) was determined in post processing using a first order polynomial fit of the calculated heat flux $q = UI/A_F$, where A_F is the measured foil area. The color evolution of the liquid crystals was recorded with a color CCD camera at a frame rate of 15 *Hz*, the spatial resolution of the observed area varied between 4.25-4.9 $pixel/mm$ depending on the distance of the target plate (Z/D).

3.4. Uncertainty calculation

The experimental uncertainties shown in the results were calculated based on the method of small perturbations, which uses the root sum square technique to combine single uncertainty terms of the measured parameters to estimate the overall uncertainty of the heat transfer coefficient [57,58].

$$\Delta h = \sqrt{\sum_{i=0}^{n} \left(\frac{\partial h}{\partial x_i} \right)^2 \Delta x_i^2} \tag{12}$$

Assuming that the uncertainty of each parameter is statistically independent and normally distributed, the error can be calculated using Eq. (12), in which we consider a 2σ (95%) confidence interval. A detailed uncertainty analysis is shown in Section 4.5.

4. Results and discussion

Tests are carried out at three Reynolds numbers (20000, 30000, 40000) at jet-to-plate distances Z/D between 4 and 10. The measured pressure drop across the orifice varied between ($\Delta p \approx$340-1350*Pa*) depending on the Reynolds number (20000–40000). The data reduction consists in the determination of the Nusselt number as a function of the radial position from the stagnation point; for this, pixels at a common distance r/D from the stagnation point are averaged. The benefit of this averaging is that the results are smoother and devoid of the noise associated with the numerical noise of the video camera that can affect the determination time at which the maximum intensity of the liquid crystal color occurs. It is to be noted, however, that results show an excellent uniformity at a constant radial distance (see Appendix C).

4.1. Reynolds variation

Fig. 4 shows results for the case Z/D=6 obtained with a rate of increase of the heat flux (q_0) equal to 50 $W/m^2 s$. The results are in very good agreement with the correlation of Goldstein and Franchett [24]. Only near the stagnation point a discrepancy can be observed. This can be attributed to the lateral conduction in the foil, which is expected to be maximal at the stagnation point, and to the chamfer of the jet hole, which can have an impact on the jet velocity profile which in turn can affect the development of the jet shear layer. The Reynolds number scaling of the heat transfer is found to be consistent with the correlation, which assumes that Nu scales with $Re^{0.7}$; the curves for the three Reynolds numbers investigated are superposed in the graph of Fig. 4, which shows Nusselt number normalized by $Re^{0.7}$

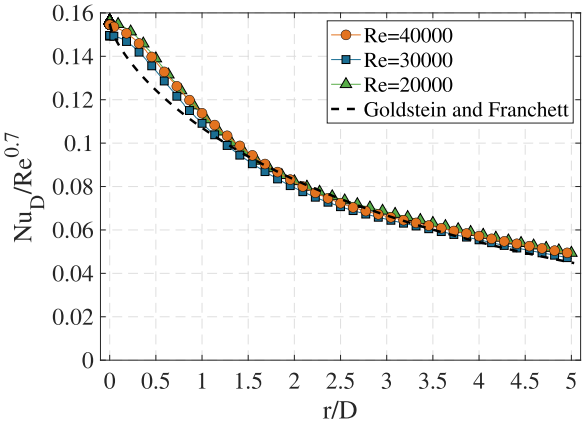

Fig. 4. Normalized Nusselt number as a function of the radial distance for Z/D=6 at various Reynolds numbers and comparison with the correlation [24]. A ramp slope q_0 of 50 $W/m^2 s$ has been used.

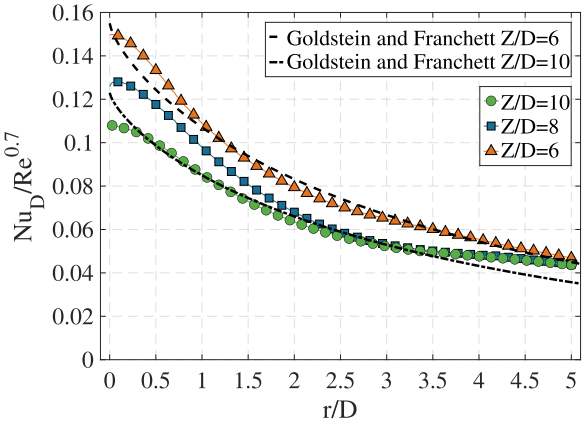

Fig. 5. Normalized Nusselt number as a function of the radial distance for various jet-to-plate distances Z/D at Re=30000, and comparison with the correlation [24]. A ramp slope q_0 of 50 $W/m^2 s$ has been used.

4.2. Jet-to-plate distance variation

In Fig. 5, results at three jet-to-plate distances are shown for Re=30000 and q_0=50 $W/m^2 s$. For two of the configurations, namely Z/D=6 and Z/D=10, results are compared with the correlation used as reference. For the case Z/D=8, however, the correlation is not available, since the scaling parameter (*A*, in reference [24]) is only defined at certain distances.

Results at Z/D=10 are in good agreement with the correlation; similarly to the Z/D=6 case, the stagnation point heat transfer is slightly lower than the correlation. For the case Z/D=8, the heat transfer level at the stagnation point is between the other two cases, as expected. At higher radial distances, however, results are shifted to similar levels as the case Z/D=10. Note that for radial distances r/D greater than 3.5, the entrainment effect correlation used [46] does not depend on the jet to plate distance Z/D, which can lead to increased uncertainty in the adiabatic wall temperature determination. Also the pixel averaging of the results for common r/D distances is based on fewer points with increasing r/D, due to the rectangular geometry of the area which is examined (Fig. 2). At

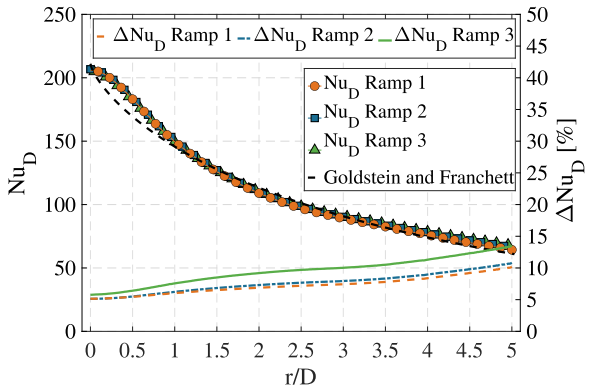

Fig. 6. Nusselt number values for the case Z/D=6 and Re=30000 with three different rates of increase of the surface heat flux, and 2σ accuracy expressed as a percentage of the local Nu_D (right axis).

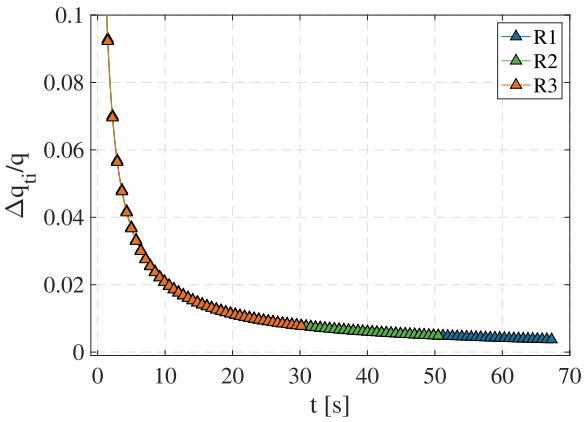

Fig. 7. Time evolution of the thermal inertia of the foil, relative to the applied heat flux for the position r/D=5 at Z/D=6 and Re=30000. Ramp 1, 2, 3 have a slope of 50, 75, and 150 W/m^2s, respectively.

higher radial distances, all cases show similar heat transfer, which is in agreement with the literature [59] and could be expected in the wall jet region.

4.3. Influence of the ramp slope

The advantage of the linearly varying heat flux method over the constant heat flux is the freedom in choosing the heat flux value, or more accurately, the rate of increase of the heat flux, provided that the total experiment time is consistent with the semi-infinite condition assumed in the solution of the heat conduction equation.

In Fig. 6, results for the case Z/D=6 at Re=30000 with three different heat flux slopes are presented: 50 $W/m^2\,s$ (ramp 1), 75 $W/m^2\,s$ (ramp 2), and 150 $W/m^2\,s$ (ramp 3). Results are independent of the ramp slope chosen. While this is obviously expected, it allows to confirm the consistency of the method. In the same figure, the result accuracy, determined with the same approach as Eq. (12), is plotted; the accuracy of the method increases when reducing the rate of increase of the heat flux, especially in the wall jet region, where the 2σ error can be reduced from 13.5% to 10% (see next sections for details on the uncertainty sources). A further reduction of the heat flux slope, however, does not improve much in terms of accuracy, as can be inferred from the similar accuracy of ramp 2 and ramp 3.

4.4. Thermal inertia of the foil and lateral conduction

To estimate the thermal inertia of the foil and its effect on the results, the experimental data are post-processed as follows: a) the temperature evolution of the surface during the experiment is computed using Eq. (6) with the experimentally determined h value; b) the time evolution of the heat flux absorbed by the foil during the experiment is computed using the equation

$$q_{ti} = \rho_s c_p \frac{dT}{dt}\delta \tag{13}$$

where δ is the thickness of the foil (see Fig. 3); c) q_{ti} can be expressed as a percentage of the applied heat flux. In this case, we consider the jet temperature to be equal to the ambient temperature T_0, to better evaluate the method itself.

Fig. 7 shows the heat flux absorbed by the foil during the experiment, expressed as a function of the instantaneous applied heat flux, for a point in the wall jet region (r/D=5). This is the location where the thermal inertia shows the greatest influence on the results, since the temperature increases the fastest.

The thermal energy absorbed by the foil is high, relative to the applied heat flux, for the first few seconds of the experiment. This is due to the fact that the applied heat flux is low at the beginning of the experiment, since it is linearly increased. The absorbed heat then quickly drops below 1% of the applied heat flux. Interestingly, the absorbed heat relative to the applied heat does not depend on the ramp slope; this can be deduced by the superposed lines in Fig. 7. Subtracting the thermal inertia to the applied heat flux gives an insight into the effect thermal inertia has on the results. A linear fit of the modified heat flux has a very similar slope as the applied heat flux but with an intercept at -25 W/m^2 instead of 0. This is similar to a shift in the time of the start of the experiment of $25/q_0$ seconds. As discussed in the next section (see Table 1), the error due to the uncertainty of the time value is very small, which means that the effect of thermal inertia can be neglected.

Due to the much higher thermal diffusivity of the metal foil compared to the PMMA material, the evaluation of the lateral conduction is mainly relevant for the foil. The evaluation is performed by post-processing the experimental data: after finding the temperature evolution at each radial location as a function of time using Eq. (6), the second derivative of the temperature as a function of the radial coordinate can be obtained numerically. A presmoothing of the heat transfer coefficient might be necessary to reduce the noise of d^2T/dr^2. Finally, the lateral conduction can be computed with the following formula:

$$q_l = k\frac{d^2T}{dr^2}\delta \tag{14}$$

In Fig. 8 the ratio of the lateral conduction to the applied heat flux is shown as a function of time for the case Z/D=6 at the stagnation point, which is where lateral conduction is expected to be maximal. The lateral conduction in the foil is maximal at the end of the experiment for the slow ramp case, and its value is approximately 0.3% of the applied heat flux. This value is small enough for the lateral conduction to be neglected.

4.5. Experimental uncertainties

Table 1 shows the calculated individual components contributing to the overall uncertainty of the heat transfer coefficient at Z/D=6 and Re=30000 for a heat flux slope of 50 $W/m^2\,s$. The error at the stagnation point is 6%, and 9% in low heat transfer regions, which is similar to the state of the art for the heater mesh method [35].

At the stagnation point, the overall uncertainty is dominated by the uncertainty on the entrainment correlation, by the ramp slope and by the thermal properties of the solid (thermal conductivity,

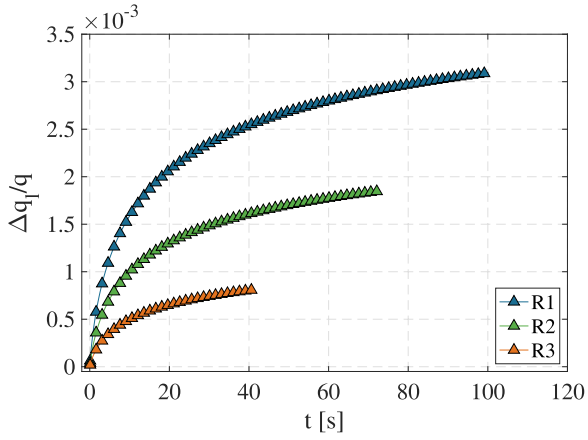

Fig. 8. Time evolution of the lateral conduction relative to the applied heat flux at the stagnation point for the case Z/D=6 and Re=30000, for the three heat flux ramps.

Table 1
Detailed uncertainties for Re=30000 Z/D=6.

	Error	High-h 350 $W/(m^2\,K)$	Low-h 120 $W/(m^2\,K)$
T_0	$\pm 0.1K$	0.06%	0.20%
T_g	$\pm 0.1K$	0.10%	0.01%
T_{LC}	$\pm 0.1K$	0.30%	0.13%
q_0	$\pm 0.5W/m^2s$	1.15%	1.61%
η	$\pm 4.3\%$	3.02%	0.16%
α	$\pm 7.5\%$	0.42%	1.63%
k	$\pm 7.5\%$	1.00%	5.04%
z	$\pm 10^{-5}m$	0.08%	0.09%
t_{LC}	$\pm 0.0667s$	0.01%	0.01%
Δh		6.14%	8.88%

thermal diffusivity). If the jet flow and the surrounding air were at the same temperature, the entrainment correlation would not be required and the uncertainty at the stagnation would be reduced by half.

In low heat transfer regions, the uncertainty is mainly due to the thermal properties, and to a minor extent to the ramp slope.

The repeatability of the experiments was good, with variations of the results always below 2%. Compared to the state of the art for the transient heater mesh method (e.g. [53]), in which the experiment is driven by a step change of the flow temperature, the method presented here achieves a 50% reduction of the uncertainty in high heat transfer regions and similar accuracy in low heat transfer regions. This increased accuracy is valuable for the accurate estimation of the overall heat transfer of established cooling solutions like arrays of impingement jets, which depend heavily on the peak heat transfer achieved at the stagnation point of the jets.

5. Conclusion

This study presented an improved experimental technique using heater foils for the determination of convective heat transfer coefficients with high resolution using transient experiments. A linearly increasing heat flux is applied on the surface of interest and narrow-bandwidth liquid crystals are used to monitor the surface temperature. This is similar to some methods in which the flow temperature is varying during the experiment. To the authors' knowledge, this is the first time a time-varying surface heat flux is applied for the evaluation of the heat transfer. The technique has been used for the case of a single jet impinging on a flat plate for a range of Reynolds numbers and jet-to-plate distances, and validated by comparing the results to the literature. The technique allows to decrease the uncertainty of the heat transfer measurements, especially in the low heat transfer region, compared to the more classical step-heating approach; this is due to the almost linear increase of the surface temperature that can be achieved with the time varying heat flux, compared to the asymptotic evolution of the step-heating method. The uncertainty of the thermal properties of the material are the major contributors of the overall uncertainty in the determination of the heat transfer coefficients. This is confirmed by the excellent repeatability of the experiments (under 2% variation between runs), which implies that the systematic error due to the uncertainty on the thermal properties of the plate is the dominating factor.

Declaration of Competing Interest

The authors declare that they have no known competing financial interests or personal relationships that could have appeared to influence the work reported in this paper.

CRediT authorship contribution statement

Julian Schmid: Conceptualization, Methodology, Validation, Software, Investigation, Writing – original draft, Writing – review & editing, Visualization. **Michele Gaffuri:** Conceptualization, Methodology, Validation, Software, Writing – original draft, Writing – review & editing, Investigation, Visualization. **Alexandros Terzis:** Funding acquisition, Supervision, Software, Writing – review & editing. **Peter Ott:** Funding acquisition, Supervision, Writing – review & editing, Resources. **Jens von Wolfersdorf:** Supervision, Methodology, Writing – review & editing.

Acknowledgements

The authors acknowledge the reviewers and editor for their contribution in improving the quality and clarity of the paper.

Appendix A. Velocity profiles

Fig. A.9 shows the velocity profiles, measured by a Pitot probe, used to derive the discharge coefficient of the nozzle.

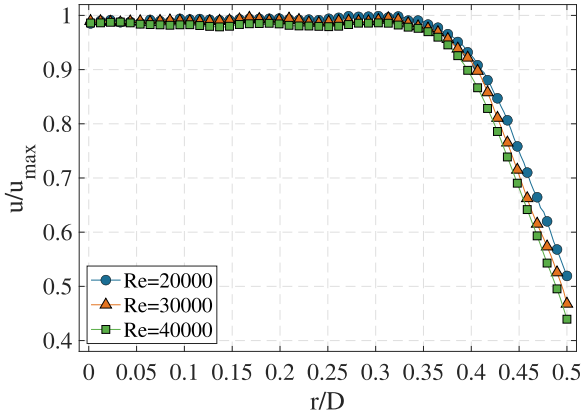

Fig. A.9. Traversed velocity profiles for different Reynolds numbers.

Appendix B. Derivation of the semi-infinite model with linearly increasing surface heat flux

The one-dimensional heat conduction equation is considered:

$$\frac{\partial^2 T(z,t)}{\partial z^2} = \frac{1}{\alpha}\frac{\partial T(z,t)}{\partial t} \tag{B.1}$$

with the following initial condition (IC) and boundary conditions (BC).

IC: The plate is initially at ambient temperature:

$$T(z, t=0) = T_0 \tag{B.2}$$

BC1: The semi-infinite boundary condition

$$T(z \to \infty, t) = T_0 \tag{B.3}$$

BC2: The surface boundary condition

$$-k\frac{\partial T(0, t>0)}{\partial z} - h[T_{aw} - T(0,t)] = q_0 t \tag{B.4}$$

In case the jet temperature is not at the same temperature as the ambient ($T_g \neq T_0$), the entrainment effect needs to be considered. Using the definition of [46], the entrainment effect is defined as:

$$\eta = \frac{T_{aw} - T_r}{T_g - T_0} \tag{B.5}$$

where T_r is the recovery temperature. Assuming a recovery factor of $r = 1$ as in [47] and small Ma numbers, T_r in Eq. (B.5) can be assumed to be equal to T_0.

Combining Eqs. (B.4) and (B.5), and rearranging:

$$-k\frac{\partial T(0, t>0)}{\partial z} + h(T(0,t)) - q_0 \cdot t = hT_0 - \eta h[T_0 - T_g] \tag{B.6}$$

To solve Eq. (B.1) one can move to the Laplace space. The Laplace equivalent of Eq. (B.1) is the following:

$$\frac{\partial^2 \overline{T}}{\partial x^2} - \frac{1}{\alpha} s\overline{T} = -\frac{1}{\alpha} T_0 \tag{B.7}$$

and the boundary condition (B.4):

$$-k\frac{\partial \overline{T}(0, s>0)}{\partial z} + h(\overline{T}(0,s)) - \frac{q_0}{s^2} = \frac{hT_0}{s} - \frac{\eta h[T_0 - T_g]}{s} \tag{B.8}$$

The general solution of Eq. (B.7) is the sum of the general solution of the homogeneous portion of the equation and a particular solution of the non-homogeneous problem:

$$\overline{T} = \overline{T}_H + \overline{T}_{NH} = C_1 e^{\sqrt{\frac{s}{\alpha}}z} + C_2 e^{-\sqrt{\frac{s}{\alpha}}z} + \frac{T_0}{s} \tag{B.9}$$

where T_0/s is a solution of the non-homogeneous problem. The constant C_1 must be 0, because T, and thus $\overline{T}$, must be bounded as $x \to \infty$. The constant C_2 can be determined by noting that Eq. (B.9) has to fulfill the boundary condition (B.8).

$$C_2 = \frac{\frac{h}{k}(T_0 - \eta(T_0 - T_g) - T_0)}{s(\sqrt{\frac{s}{\alpha}} + \frac{h}{k})} + \frac{q_0/k}{s^2(\sqrt{\frac{s}{\alpha}} + \frac{h}{k})} \tag{B.10}$$

which, inserted into (B.9), gives the solution in Laplace space:

$$\overline{T} = \frac{-\frac{h}{k}\eta(T_0 - T_g)}{s(\sqrt{\frac{s}{\alpha}} + \frac{h}{k})} e^{-\sqrt{\frac{s}{\alpha}}z} + \frac{q_0/k}{s^2(\sqrt{\frac{s}{\alpha}} + \frac{h}{k})} e^{-\sqrt{\frac{s}{\alpha}}z} + \frac{T_0}{s} \tag{B.11}$$

To get the solution in the temporal space, the inverse transform of each one of the three terms on the right hand side of Eq. (B.11), (T_1, T_2, and T_3 in the following) must be found. For better overview, in the following the terms $a = \frac{z}{2\sqrt{\alpha t}}$, $b = \frac{hz}{k} + \alpha t \frac{h^2}{k^2}$ and $c = \frac{h}{k}\sqrt{\alpha t}$ are used.

The first term corresponds to the convection due to the difference between the flow temperature and the initial plate temperature. The inverse Laplace transform is obtained from Carslaw and Jaeger [48] p. 72 and reads:

$$T_1(z,t) = -\eta(T_0 - T_g)\left[\text{erfc}(a) - e^b \text{erfc}(a+c)\right] \tag{B.12}$$

The second term corresponds to the effect of the applied heat flux. The inverse transform can be found using expression 16 in the Appendix 5 of [48]. To get the same form as in [48], one can perform the substitution $g = \sqrt{\frac{s}{\alpha}}$:

$$\overline{T}_2(z,s) = \frac{\frac{q_0}{k/\alpha^2} e^{gz}}{g^4(g + \frac{h}{k})} \tag{B.13}$$

The inverse Laplace transform of (B.13) reads:

$$T_2(z,t) = \frac{q_0}{k\alpha^2}\left[\frac{\alpha}{\left(-\frac{h}{k}\right)^3} e^b \text{erfc}\{a+c\} - \frac{\alpha}{\left(-\frac{h}{k}\right)^3}\sum_{r=0}^{2}(-2c)^r i^r \text{erfc}\{a\}\right] \tag{B.14}$$

Term three is simply the initial temperature, and the inverse transform is straightforward:

$$T_3(z,t) = T_0 \tag{B.15}$$

Combining Eqs. (B.12), (B.14) and (B.15) leads to the final solution:

$$\begin{aligned} T(z,t) - T_0 = &-\eta(T_0 - T_g)\left[\text{erfc}(a) - e^b \text{erfc}(a+c)\right] \\ &+ \frac{q_0}{k\alpha^2}\left[\frac{\alpha}{\left(-\frac{h}{k}\right)^3} e^b \text{erfc}(a+c) - \frac{\alpha}{\left(-\frac{h}{k}\right)^3}\sum_{r=0}^{2}(-2c)^r i^r \text{erfc}(a)\right] \end{aligned} \tag{B.16}$$

In Eqs. (B.14) and (B.16), the term $i^r\text{erfc}(a)$ denotes the rth successive integration of the complementary error function, which can be defined iteratively as follows (see Appendix 2 in [48]):

$$i^n \text{erfc}(x) = \int_x^\infty i^{n-1}\text{erfc}(\xi)\, d\xi \tag{B.17}$$

with

$$i^0 \text{erfc}(x) = \text{erfc}(x) \tag{B.18}$$

For n=1,2, Eq. (B.17) can be solved by integrating by parts, leading to the following expressions:

$$i^1 \text{erfc}(x) = \frac{1}{\sqrt{\Pi}} \exp(-x^2) - x\ \text{erfc}(x) \tag{B.19}$$

$$i^2 \text{erfc}(x) = \frac{1}{4}[\text{erfc}(x) - 2x(i^1\text{erfc}(x))] \tag{B.20}$$

Appendix C. Nusselt number distribution

Fig. C.10 shows an example of Nusselt number contours for the area where heat transfer coefficients can be evaluated. The circular contours show a good circumferential uniformity of the results.

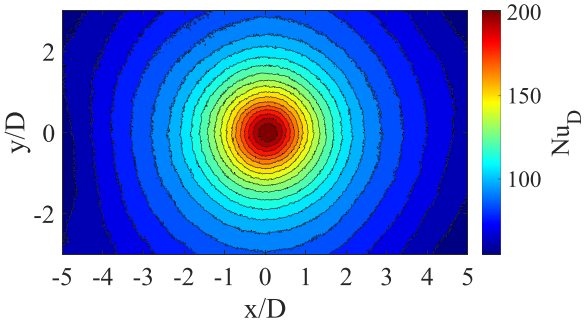

Fig. C.10. Nusselt number distribution of the surface to be examined for the case Re=30000, Z/D=6.

Appendix D. Nusselt number correlation

With the experimental data available, the correlation of Goldstein and Franchett [24], which covers only specific jet-to-plate distances, can be extended to arbitrary distances in the interval $4 \leq Z/D \leq 10$ for a jet perpendicularly impinging a surface.

For normal jets, the correlation in [24] takes the form:

$$\frac{Nu}{Re^{0.7}} = A \exp\left(-0.37(r/D)^{0.75}\right) \tag{D.2}$$

The parameter A depends on the jet-to-plate distance Z/D, and is defined only at 3 distances. To extend the correlation to arbitrary Z/D, Eq. (D.2) is fitted to the data; in this way, the value A that best fits the data is obtained for each experiment. A quadratic function of Z/D provides a good fit of the parameter *A* for the available data:

$$A = -0.0012(Z/D)^2 + 0.012(Z/D) + 0.1267 \tag{D.3}$$

Table D.2 shows a comparison of the value of parameter A found using Eq. (D.3) with the values given in [24]; there is a good agreement at these distances. Goldstein and Franchett predict slightly higher values at Z/D=4 than at Z/D=6, while Eq. (D.3) predicts the same level at both distances, with a maximum at Z/D=5. Nusselt number levels, however, are almost constant for Z/D in the range [4, 6], as is also noted in [24]. One can thus conclude that the extension of the correlation proposed here is consistent with the original correlation.

Table D.2
Values of parameter A predicted by Eq. (D.3) and by Goldstein and Franchett [24].

Z/D	A (present work)	A (Goldstein and Franchett)
4	0.156	0.159
6	0.156	0.155
10	0.127	0.123

References

[1] C. Waidmann, R. Poser, M. Ghring, J. von Wolfersdorf, First operation of a rotating test rig for transient thermochromic liquid crystal heat transfer experiments, XXIV Biannual Symposium on Measuring Techniques in Turbomachinery, 2018.

[2] M. Fiebig, A. Valencia, N. Mitra, Wing-type vortex generators for fin-and-tube heat exchangers, Exp. Therm. Fluid Sci. 7 (4) (1993) 287–295, doi:10.1016/0894-1777(93)90052-K.

[3] R. Poser, J. von Wolfersdorf, Liquid crystal thermography for transient heat transfer measurements in complex internal cooling systems, Heat Transf. Res. 42 (2009) 1–13, doi:10.1615/ICHMT.2009.HeatTransfGasTurbSyst.510.

[4] G. Vogel, A. Graf, J. von Wolfersdorf, B. Weigand, A novel transient heater-foil technique for liquid crystal experiments on film-cooled surfaces, J. Turbomach. 125 (3) (2003) 529–537, doi:10.1115/1.1578501.

[5] S.V. Ekkad, S. Ou, R.B. Rivir, A transient infrared thermography method for simultaneous film cooling effectiveness and heat transfer coefficient measurements from a single test, J. Turbomach. 126 (4) (2004) 597–603, doi:10.1115/1.1791283.

[6] M. Jonsson, D. Charbonnier, P. Ott, J. von Wolfersdorf, Application of the transient heater foil technique for heat transfer and film cooling effectiveness measurements on a turbine vane endwall, in: Proceedings of ASME Turbo Expo: Power for Land, Sea and Air, Berlin, Germany, 2008, pp. 443–453, doi:10.1115/GT2008-50451.

[7] D.C. Reda, M.C. Wilder, D.J. Farina, G. Zilliac, New methodology for the measurement of surface shear stress vector distributions, AIAA J. 35 (4) (1997) 608–614, doi:10.2514/2.165.

[8] D.R. Buttsworth, S.J. Elston, T.V. Jones, Directional sensitivity of skin friction measurements using nematic liquid crystal, Meas. Sci. Technol. 9 (11) (1998) 1856–1865, doi:10.1088/0957-0233/9/11/011.

[9] J. Simonich, R. Moffat, New technique for mapping heat-transfer coefficient contours, Rev. Sci. Instrum. 53 (5) (1982) 678–683, doi:10.1063/1.1137041.

[10] J. Baughn, M. Hoffman, D. Makel, Improvements in a new technique for measuring and mapping heat transfer coefficients, Rev. Sci. Instrum. 57 (4) (1986) 650–654, doi:10.1063/1.1138883.

[11] R.J. Moffat, Some experimental methods for heat transfer studies, Exp. Therm. Fluid Sci. 3 (1) (1990) 14–32, doi:10.1016/0894-1777(90)90098-R.

[12] K.H. Platzer, C. Hirsch, D.E. Metzger, S. Wittig, Computer-based areal surface temperature and local heat transfer measurements with thermochromic liquid crystals (TLC), Exp. Fluids 13 (1) (1992) 26–32, doi:10.1007/BF00208071.

[13] P.W. Giel, D.R. Thurman, G.J. Van Fossen, S.A. Hippensteele, R.J. Boyle, Endwall heat transfer measurements in a transonic turbine cascade, J. Turbomach. 120 (2) (1998) 305–313, doi:10.1115/1.2841407.

[14] H. Ay, J. Jang, J.-N. Yeh, Local heat transfer measurements of plate finned-tube heat exchangers by infrared thermography, Int. J. Heat Mass Transf. 45 (20) (2002) 4069–4078, doi:10.1016/S0017-9310(02)00132-1.

[15] G.M. Carlomagno, G. Cardone, Infrared thermography for convective heat transfer measurements, Exp. Fluids 49 (2010), doi:10.1007/S00348-010-0912-2.

[16] M. Modak, K. Garg, S. Srinivasan, S.K. Sahu, Theoretical and experimental study on heat transfer characteristics of normally impinging two dimensional jets on a hot surface, Int. J. Therm. Sci. 112 (2017) 174–187, doi:10.1016/j.ijthermalsci.2016.10.009.

[17] J.J. Lee, J.C. Dutton, A.M. Jacobi, Application of temperature-sensitive paint for surface temperature measurement in heat transfer enhancement applications, J. Mech. Sci. Technol. 21 (8) (2007) 1253–1262, doi:10.1007/BF03179042.

[18] C. He, Y. Liu, Jet impingement heat transfer of a lobed nozzle: measurements using temperature-sensitive paint and particle image velocimetry, Int. J. Heat Fluid Flow 71 (2018) 111–126, doi:10.1016/j.ijheatfluidflow.2018.03.017.

[19] F. Satta, G. Tanda, Measurement of local heat transfer coefficient on the endwall of a turbine blade cascade by liquid crystal thermography, Exp. Therm. Fluid Sci. 58 (2014) 209–215, doi:10.1016/j.expthermflusci.2014.07.005.

[20] D. Sarkar, A. Jain, R. Goldstein, S. V., Corrections for lateral conduction error in steady state heat transfer measurements, Int. J. Therm. Sci. 109 (2016) 413–423, doi:10.1016/j.ijthermalsci.2016.05.031.

[21] L. Ratto, F. Satta, G. Tanda, An experimental and numerical study of endwall heat transfer in a turbine blade cascade including tangential heat conduction analysis, Heat Mass Transf. 54 (6) (2018) 1627–1636, doi:10.1007/s00231-017-2254-6.

[22] C. Hoogendoorn, The effect of turbulence on heat transfer at a stagnation point, Int. J. Heat Mass Transf. 20 (12) (1977) 1333–1338, doi:10.1016/0017-9310(77)90029-1.

[23] T.H. Van der Meer, Stagnation point heat transfer from turbulent low Reynolds number jets and flame jets, Exp. Therm. Fluid Sci. 4 (1) (1991) 115–126, doi:10.1016/0894-1777(91)90025-M.

[24] R.J. Goldstein, M.E. Franchett, Heat transfer from a flat surface to an oblique impinging jet, J. Heat Transf. 110 (1) (1988) 84–90, doi:10.1115/1.3250477.

[25] T.V. Jones, S.A. Hippensteele, High-Resolution Heat-Transfer-Coefficient Maps Applicable to Compound-Curve Surfaces using Liquid Crystals in a Transient Wind Tunnel, NASA Technical Memorandum, NASA, 1988.

[26] S.V. Ekkad, J.-C. Han, A transient liquid crystal thermography technique for gas turbine heat transfer measurements, Meas. Sci. Technol. 11 (7) (2000) 957–968, doi:10.1088/0957-0233/11/7/312.

[27] U. Ansu, S.C. Godi, A. Pattamatta, C. Balaji, Experimental investigation of the inlet condition on jet impingement heat transfer using liquid crystal thermography, Exp. Therm. Fluid Sci. 80 (2017) 363–375, doi:10.1016/j.expthermflusci.2016.08.028.

[28] D.L. Schultz, T. Jones, Heat-Transfer Measurements in Short-Duration Hypersonic Facilities., Technical Report, Advisory Group for Aerospace Research and Development, 1973.

[29] G. Vogel, B. Weigand, A new evaluation method for transient liquid crystal experiments, in: Proceedings of the 35th National heat Transfer Conference, 2001.

[30] J.P.C.W. Ling, P.T. Ireland, L. Turner, A technique for processing transient heat transfer, liquid crystal experiments in the presence of lateral conduction, J. Turbomach. 126 (2) (2004) 247–258, doi:10.1115/1.1740777.

[31] J.R. Kingsley-Rowe, G.D. Lock, J. Michael Owen, Transient heat transfer measurements using thermochromic liquid crystal: lateral-conduction error, Int. J. Heat Fluid Flow 26 (2) (2005) 256–263, doi:10.1016/j.ijheatfluidflow.2004.08.011.

[32] J. von Wolfersdorf, Influence of lateral conduction due to flow temperature variations in transient heat transfer measurements, Int. J. Heat Mass Transf. 50 (5) (2007) 1122–1127, doi:10.1016/j.ijheatmasstransfer.2006.06.049.

[33] S. Brack, R. Poser, J. von Wolfersdorf, An approach to consider lateral heat conduction effects in the evaluation process of transient heat transfer measurements using TLC, Int. J. Therm. Sci. 107 (2016) 289–302, doi:10.1016/j.ijthermalsci.2016.03.028.

[34] D.E. Metzger, D.E. Larson, Use of melting point surface coatings for local convection heat transfer measurements in rectangular channel flows with 90-deg turns, J. Heat Transf. 108 (1) (1986) 48–54, doi:10.1115/1.3246903.

[35] A. Terzis, P. Ott, J. von Wolfersdorf, B. Weigand, M. Cochet, Detailed heat transfer distributions of narrow impingement channels for cast-in turbine airfoils, J. Turbomach. 136 (9) (2014), doi:10.1115/1.4027679.

[36] H. Ma, Z. Wang, L. Wang, Q. Zhang, Y. Bao, Ramp heating in high-Speed transient thermal measurement with reduced uncertainty, J. Propul. Power 32 (5) (2016) 1190–1198, doi:10.2514/1.B35803.

[37] J.S. Kwak, Comparison of analytical and superposition solutions of the transient liquid crystal technique, J. Thermophys. Heat Transf. 22 (2) (2008) 290–295, doi:10.2514/1.34274.

[38] P.J. Newton, Y. Yan, N.E. Stevens, S.T. Evatt, G.D. Lock, J. Owen, Transient heat transfer measurements using thermochromic liquid crystal. Part 1: an improved technique, Int. J. Heat Fluid Flow 24 (1) (2003) 14–22, doi:10.1016/S0142-727X(02)00206-0.

[39] J. von Wolfersdorf, R. Hoecker, T. Sattelmayer, A hybrid transient step-heating heat transfer measurement technique using heater foils and liquid-crystal thermography, J. Heat Transf. 115 (2) (1993) 319–324, doi:10.1115/1.2910682.
[40] M. Gaffuri, A. Terzis, P. Ott, S. Retzko, M. Henze, Evaluation of heat transfer coefficients for an impingement cooling cascade: experimental challenges and preliminary results, XXIV Biannual Symposium on Measuring Techniques in Turbomachinery, 2018.
[41] D.R.H. Gillespie, Z. Wang, P.T. Ireland, S.T. Kohler, Full surface local heat transfer coefficient measurements in a model of an integrally cast impingement cooling geometry, J. Turbomach. 120 (1) (1998) 92–99, doi:10.1115/1.2841394.
[42] A. Terzis, J. von Wolfersdorf, B. Weigand, P. Ott, Thermocouple thermal inertia effects on impingement heat transfer experiments using the transient liquid crystal technique, Meas. Sci. Technol. 23 (11) (2012), doi:10.1088/0957-0233/23/11/115303.
[43] A.R.A. Talib, A.J. Neely, P.T. Ireland, A.A. Mullender, A novel liquid crystal image processing technique using multiple gas temperature steps to determine heat transfer coefficient distribution and adiabatic wall temperature, J. Turbomach. 126 (4) (2004) 587–596, doi:10.1115/1.1776585.
[44] D. Ai, P.P. Ding, P.H. Chen, Selection criterion of injection temperature pair for transient liquid crystal thermography on film cooling measurements, Int. J. Heat Mass Transf. 44 (7) (2001) 1389–1399, doi:10.1016/S0017-9310(00)00153-8.
[45] B. Facchini, M. Surace, Impingement cooling for modern combustors: experimental analysis of heat transfer and effectiveness, Exp. Fluids 40 (4) (2006) 601–611, doi:10.1007/s00348-005-0100-y.
[46] R.J. Goldstein, K.A. Sobolik, W.S. Seol, Effect of entrainment on the heat transfer to a heated circular air jet impinging on a flat surface, J. Heat Transf. 112 (1990) 608–611, doi:10.1115/1.2910430.
[47] J.W. Baughn, A.E. Hechanova, X. Yan, An experimental study of entrainment effects on the heat transfer from a flat surface to a heated circular impinging jet, J. Heat Transf. 113 (4) (1991) 1023–1025, doi:10.1115/1.2911197.
[48] H.S. Carslaw, J.C. Jaeger, Conduction of Heat in Solids, vol. 2, second ed., Oxford at the Clarendon press, 1959.
[49] S.A. Hippensteele, L.M. Russell, F.S. Stepka, Evaluation of a method for heat transfer measurements and thermal visualization using a composite of a heater element and liquid crystals, J. Heat Transf. 105 (1) (1983) 184–189, doi:10.1115/1.3245539.
[50] J.E. Mayhew, J.W. Baughn, A.R. Byerley, The effect of freestream turbulence on film cooling adiabatic effectiveness, Int. J. Heat Fluid Flow 24 (5) (2003) 669–679, doi:10.1016/S0142-727X(03)00081-X.
[51] L.V. Tran, J.S. Kapat, Coupled zero-dimensional/one-dimensional model for hybrid heat transfer measurements, J. Thermophys. Heat Transf. 28 (2) (2014) 236–250, doi:10.2514/1.T4066.
[52] M. Fénot, X.T. Trinh, E. Dorignac, Flow and heat transfer of a compressible impinging jet, Int. J. Therm. Sci. 136 (2019) 357–369, doi:10.1016/j.ijthermalsci.2018.10.035.
[53] A. Terzis, S. Bontitsopoulos, P. Ott, J. von Wolfersdorf, A.I. Kalfas, Improved accuracy in jet impingement heat transfer experiments considering the layer thicknesses of a triple thermochromic liquid crystal coating, J. Turbomach. 138 (2) (2015), doi:10.1115/1.4031786.
[54] S. Schulz, S. Brack, A. Terzis, J. von Wolfersdorf, P. Ott, On the effects of coating thickness in transient heat transfer experiments using thermochromic liquid crystals, Exp. Therm. Fluid Sci. 70 (2016) 196–207, doi:10.1016/j.expthermflusci.2015.08.011.
[55] C. Waidmann, R. Poser, J. von Wolfersdorf, Application of thermochromic liquid crystal mixtures for transient heat transfer measurements, in: 10th European Conference on Turbomachinery Fluid dynamics & Thermodynamics, European Turbomachinery Society, 2013.
[56] O. Caggese, G. Gnaegi, G. Hannema, A. Terzis, P. Ott, Experimental and numerical investigation of a fully confined impingement round jet, Int. J. Heat Mass Transf. 65 (2013) 873–882, doi:10.1016/j.ijheatmasstransfer.2013.06.043.
[57] S.J. Kline, Describing uncertainty in single sample experiments, Mech. Eng. 75 (1) (1953) 3–8.
[58] R. Moffat, Describing the uncertainties in experimental results, Exp. Therm. Fluid Sci. 1 (1988) 3–17, doi:10.1016/0894-1777(88)90043-X.
[59] J.W. Baughn, S. Shimizu, Heat transfer measurements from a surface with uniform heat flux and an impinging jet, J. Heat Transf. 111 (4) (1989) 1096–1098, doi:10.1115/1.3250776.